 doi:10.20944/preprints202208.0066.v1

Article

pH-Sensitive Polyacrylic Acid-Gated Mesoporous Silica Nanocarrier Incorporated with Calcium Ions for Controlled Drug Release

Jungwon Kong [1], Sung Soo Park [2] and Chang-Sik Ha [1,*]

[1] Department of Polymer Science and Engineering, School of Chemical Engineering, Pusan National University, Busan 46241, Republic of Korea; ggong93@naver.com (J.K.); csha@pnu.edu (C.-S.H.)
[2] Division of Advanced Materials Engineering, Dong-Eui University, Busan 47340, Republic of Korea; pss@deu.ac.kr (S.S.P.)
* Correspondence: csha@pusan.ac.kr (C.-S.H.)

Abstract: In this work, polyacrylic acid-functionalized MCM-41 was synthesized, which was further interacted with calcium ions, to realize enhanced pH-responsive nanocarrier for sustained drug release. First, mesoporous silica nanoparticles (MSNs) were prepared by the sol-gel method. Afterward, (3-trimethoxysilyl)propyl methacrylate (TMSPM) modified surface was prepared by using the post-grafting method, then polymerization of acrylic acid was proceeded. After adding calcium chloride solution, polyacrylic acid-functionalized MSNs with calcium-carboxyl ionic bonds in the polymeric layer, which can prevent the cargo from leaking out of the mesopore, were prepared. The structure and morphology of the modified nanoparticles (PAA-MSNs) were characterized by X-ray diffraction (XRD), Fourier-transform infrared (FT-IR) spectroscopy, transmission electron microscopy (TEM), and N_2 adsorption-desorption analysis, etc. The controlled release of guest molecules was studied by using 5-fluorouracil (5-FU). The drug molecules-incorporated nanoparticles showed different releasing rates under different pH conditions. It is considered that our current materials have the potential as pH-responsive targeted nanocarriers in the field of medical treatment.

Keywords: Mesoporous silica, Polyacrylic acid, Calcium ion, 5-Fluorouracil, Drug delivery

1. Introduction

Responsive materials have attracted a lot of interest in the research and industry in recent years. It can provide proper opportunities in many fields such as automotive [1], aerospace [2,3], electric devices [4], and medical applications [5-7]. Especially, this smart material's sensitiveness to specific stimuli can show positive possibilities for advances in cancer therapy [8-11]. Cancer is a disease caused by abnormal cell growth and is still the main cause of death in humans. There are several treatments available to treat cancer, but chemotherapy is one of the most commonly used cancer treatments [12]. However, present chemotherapeutic drugs have low specificity to targeted cancerous cells [13,14]. When a drug is administered to the human body, the lack of specificity of a drug molecule leads to a high-dosage regimen and causes undesired interactions of a drug with normal cells [15]. This can have a detrimental effect on a person, causing damage to healthy organs or tissues. The efficiency of treatment would be decreased and side effects will follow related to systemic toxicity. To overcome this disadvantage, many researchers have been investigating on the controlled drug delivery system (CDDS) [16,17]. Stimuli-responsive materials such as polymers [18,19], hydrogels, and many kinds of inorganic nanoparticles can be utilized in CDDS actively as a means of transport. In response to external stimuli (temperature, light irradiation, pH, redox, etc.), the release amount of the drug can be controlled more precisely than the drug without any device. In the case of cancer treatment, pH-responsive materials are gaining lots of interest because cancer tumor tissue is more acidic than normal tissue. (pH 4.0~6.0) [20]. The pH-sensitive material's delivery

Preprints (www.preprints.org) | NOT PEER-REVIEWED | Posted: 2 August 2022 doi:10.20944/preprints202208.0066.v1

system, which can do the targeted drug release at a low pH region and no response to the normal physiological environment, would be a worthy method of treatment [21-23].

Among various drug delivery systems, mesoporous silica nanoparticles (MSNs) have been the subject of interest in recent years because of their large surface area, high pore volume, tunable pore size, and chemical stability [24,25]. It has great biocompatibility and high loading capacity among other systems too. By adding a drug or other cargo inside the MSNs, it can protect them from degradation and guard them against leakage. Also, MSNs can be functionalized easily on the internal and external surface so that diverse modifications are possible to prevent premature abruption of drugs or cargos from the pore of mesoporous silica particles [26]. the size of the nanoparticle of around 100 nm makes it possible to be passed to the cells by endocytosis [27].

From the perspective of the drug delivery material, polymers having adjustable properties such as biodegradability and biocompatibility have been studied a lot as materials for drug delivery systems [28-30]. Phase-transfer polymers are sensitive to external stimuli and are continuously or discontinuously hydrated [31,32]. These polymers show a change in physical properties of external stimuli that include chemical or biochemical stimuli like pH and metabolites, and physical stimuli such as temperature, light electric field, and solvent [33,34]. However, drug-polymer conjugates have bad stability and loading capacities are low. To optimize this transport platform, we have to address these issues.

By functionalizing polymers on the surface of the mesoporous silica nanoparticles, we can obtain a hybrid nanoparticle that has high stability and loading capacity as well as adjustable properties which can make sensitive stimuli-switchable nanocarrier [24,35-38]. The connection of polymers such as polyacrylamide [39], poly(methacrylic acid) [40,41], poly(diethylaminoethyl methacrylate) [42], chitosan [43-45], poly(4-vinylpyridine) [37,46] and etc. [47] realized the pH-responsive polymer-coated mesoporous silica particles for drug delivery systems [48].

In this work, 5-fluorouracil (5-FU) encapsulated mesoporous silica delivery system matrix was prepared, which has polyacrylic acid (PAA) chains on the surface as a gatekeeper. 5-FU is an anticancer drug that can be used in the treatment of stomach cancer, pancreatic cancer, and so on. It is negatively charged and has low lipid solubility. First, MCM-41 nanoparticles were synthesized by a liquid crystal templating mechanism. Second, PAA was attached to the surface of MCM-41. PAA has low toxicity and provides more hydrophilicity to mesoporous silica materials. Furthermore, it has a carboxylic group that can make electrostatic interaction with calcium ions. By mixing calcium chloride solution with the 5-FU loaded MCM-41-PAA, metal complexes were formed by complexation between the calcium atom and carboxyl groups. That can be a barrier in a neutral and basic environment by capping the pore exits. While in an acidic environment, the interactions between carboxylate ion and calcium ion would be decreased and the release of drugs inside the pore could be possible. Preparation of drug delivery nanomatrix is presented and characterization of each step was carried out. As-made MSNs have a large surface area and pore volume to proper to be used in a carrier of drugs. The release characteristics of 5-FU were also assessed. It showed selective release amount under each different pH environment. The results indicated that its pH-responsivity is sufficiently available to apply in cancer treatment.

2. Experimental Section

2.1. Materials

Cetyltrimethylammonium bromide (CTABr, >99%), tetraethyl orthosilicate (TEOS, 98%), 3-(trimethoxysilyl)propyl methacrylate (TMSPM), toluene (anhydrous, ≥99.8%), acrylic acid, ethanol (anhydrous), potassium persulfate (KPS, ≥99%), N,N′-methylenebis(acrylamide) (MBA), calcium chloride and 5-fluorouracil (5-FU, ≥99%). All the above materials were purchased from Sigma-Aldrich. Sodium hydride (bead, 98.0%) (NaOH) and dichloromethane was purchased from Samchun Chemical. Hydrochloric acid (35%)

Preprints (www.preprints.org) | NOT PEER-REVIEWED | Posted: 2 August 2022 doi:10.20944/preprints202208.0066.v1

(HCl) was purchased from Matsunoen Chemicals Ltd. All the reagents were used without further purification.

2.2. Synthesis of MCM-41

MCM-41 nanoparticles were synthesized according to the method reported in the literature [49]. CTABr (1 g, 2.74 mmol) and NaOH (0.28 g, 7 mmol) were added to deionized (DI) water (480 g, 26.6 mol) in a 1 L round bottom (RB) flask and stirred at room temperature for 1 h to obtain a homogeneous mixture. The homogeneous mixture was heated for 30 min to achieve a stabilized temperature (80 °C) with constant stirring. Then TEOS (5 mL, 22.39 mmol) was added dropwise to the solution and the total mixture was stirred continually at 80 °C for two more hours. The molar composition of the total mixture was 1.0 SiO_2:0.12 CTABr:0.31 NaOH:1188 H_2O. The obtained product was isolated, washed with ethanol several times by centrifugation, and dried in an oven at 70 °C for 24 h. The resulting product was named as 'As-synthesized MCM-41'.

2.3. Functionalization with double bond groups (MCM-41-TMSPM)

For the removal of water bonded with silanol groups on the surface of nanoparticles, As-synthesized MCM-41 was degassed at 110 °C for more than 12 h under vacuum. 2 g of the degassed As-synthesized MCM-41 was transferred to a 100 ml round bottom flask with 50 ml of anhydrous toluene. After stirring for 1 min at room temperature, 2 ml of TMSPM was added to the system. The mixture was kept at 110 °C for 24 h with constant stirring under a nitrogen atmosphere. And the mixture was centrifugated 6 times with toluene and DCM. The resulting product was named as 'as-MCM-41-TMSPM'. After this procedure, solvent extraction was conducted to remove CTABr surfactant in the mesopores. 1.5 g of as-MCM-41-TMSPM was stirred for 12 h in 225 ml of ethanol solution containing 35 wt% HCl (4.5 ml) at 60 °C. This procedure was repeated 3 times. The obtained product was isolated and washed with toluene several times by centrifugation and dried in an oven at 70 °C for 24 h. The resulting product was named as 'MCM-41-TMSPM'.

2.4. Synthesis of polyacrylic acid-functionalized MCM-41 (MCM-41-PAA)

The functionalization of polyacrylic acid was performed by referring to the process of literature [50]. polyacrylic acid-functionalized MCM-41was prepared by free-radical polymerization of acrylic acid (AA). 0.46 g of MCM-41-TMSPM was degassed at 70 °C over 12 h under vacuum. The degassed sample was dispersed in a 40 ml deionized (DI) water : ethanol mixture (1:1 v/v) in a 250 ml round bottom flask and purged with nitrogen for 6 h for the removal of oxygen in the mesopores of MCM-41-TMSPM. In this mixture, 1.38 g of AA in 40 ml DI water : ethanol mixture (1:1 v/v) was added with 12.3 mg of MBA as a crosslinker agent. The mixture was stirred for 1 h at 80 °C under a nitrogen atmosphere. After that, 24 mg of KPS was added as an initiator agent and the total mixture was stirred for 12 h at 80 °C under a nitrogen atmosphere. The obtained product was filtered by centrifugation and washed with water, ethanol, and dichloromethane to remove the polymer physically attached to the surface of nanoparticles. The resulting product was named as 'MCM-41-PAA'.

2.5. Preparation of calcium ion interacted 5-FU loaded MCM-41-PAA matrix (Ca@MCM-41-PAA_5-FU)

The chemotherapy drug, 5-Fluorouracil (5-FU) was loaded into the MCM-41-PAA by adding the MCM-41-PAA (100 mg) in an aqueous solution of 5-FU (10 ml, 1 mg ml^{-1}) at room temperature and stirred for 24 h. Then $CaCl_2$ solution (10 ml, 0.01 M) was added and the reaction mixture was stirred for another 24 h, leading to form electrostatic interactions between Ca^{2+} and the COO^- at a pH 7.4 environment. The obtained mixture was isolated by centrifugation and washed with DI water 2 times. The resulting materials were dried in an oven at 70 °C for 12 h. The resulting product was named as 'Ca@MCM-41-

Preprints (www.preprints.org) | NOT PEER-REVIEWED | Posted: 2 August 2022 doi:10.20944/preprints202208.0066.v1

PAA_5-FU'. The loading of 5-FU in MCM-41-PAA nanocarrier was confirmed by wide-angle X-ray diffraction (WXRD) and energy-dispersive X-ray spectroscopy (EDS) and the loading amount of 5-FU was evaluated by UV-vis spectroscopy.

The 5-FU loaded MCM-41 (named as 'MCM-41_5-FU') and 5-FU loaded MCM-41-PAA (named as 'MCM-41-PAA_5-FU') without Ca^{2+} ions were prepared by the method as same as the previously mentioned one.

2.6. Drug releasing test

20 mg of MCM-41_5-FU, MCM-41-PAA_5-FU, and Ca@MCM-41-PAA_5-FU was added to 5 ml of PBS (phosphate buffer saline) solution and the dispersion was filled into a dialysis bag (cutoff molecular weight (Mw) = 1.2 kDa). The bag with dispersion was immersed in 20 ml of PBS solution of different pH (5.4, 7.4) at 37 °C in a shaking incubator. At the specific time intervals, 2 ml of external medium was taken and replaced with the same volume of new PBS buffer solution immediately. The amount of released 5-FU was calculated by measuring intensity by UV-vis spectrophotometer at 266 nm.

$$\%R_t = \frac{C_t \cdot V_1 + V_2 \cdot (C_{t-1} + C_{t-2} + \cdots + C_0)}{W_0 \cdot L} \times 100\%$$

The above equation was applied to calculate the drug release degree of samples. In this equation, C_t is the drug concentration at time interval t; $C_{t-1} + C_{t-2}$ are drug concentrations prior to time interval t ($C_0 = 0$); V_1 is the total volume of the release bath (25 ml), and V_2 is the volume extracted for UV-vis analysis (2 ml). W_1 is the initial weight of the 5-FU-loaded MSNs and L is the drug loading capacity of the MSNs_5-FU [51]. Also, calibration curves of 5-FU in DI water, and PBS buffer at different pH (pH 5.4, 7.4) were used to translate UV-vis intensity to the concentration of 5-FU in the medium.

2.7. Measurements and characterization

X-ray powder diffraction (XRD, Bruker AXS) was performed using Cu-Kα radiation (1.5418 Å) at 30 kV and 15 mA in the 2θ range, 0.5~10° (LXRD), 10~80° (WXRD). The characteristic surface functional groups were analyzed by Fourier transform infrared spectroscopy (FTIR, JASCO (FTIR-4100)) at a scanning range of 400–4000 cm^{-1} in KBr. Transmission electron microscopy (TEM, TALOS F200X) was performed at an accelerating voltage of 200 kV and Energy dispersive X-ray spectroscopy (EDS) fast signal detection was conducted. High resolution low voltage scanning electron microscopy (HRLV-SEM, JSM-7900F) was conducted at an operating voltage of 2.0 kV. Thermogravimetric analysis (TGA, TA, Q50) was carried out at a heating rate of 10 °Cmin^{-1} in nitrogen gas from 30 °C to 800 °C to measure thermal stability of samples. The adsorption/desorption isotherms of nitrogen at 77 K were measured using a Nova 4000e surface area and pore size analyzer. Before starting the measurements, each sample was outgassed for 12 h under vacuum at 343K. The pore surface area was calculated by Brunauer Emmet-Teller (BET) method and the pore size distribution curve was obtained from an analysis of the adsorption branch using the Barrette-Joynere-Halenda (BJH) method. The zeta potentials were observed by Zetasizer Nano ZS (Malvern Instruments Ltd, U.K.) at room temperature. The particle size distribution curves were also measured using a dynamic light scattering spectrophotometer (Zetasizer Nano, Malvern). Ultraviolet–visible (UV-vis) spectrophotometry (Hitachi U-2010) was used to measure the drug release rate.

3. Results and discussion

3.1. Synthesis of MCM-41 and functionalized MCM-41

Scheme 1 outlines the preparation of polyacrylic acid functionalized MCM-41 and releasing behavior of drug molecules under pH stimulus. After loading 5-FU and calcium chloride, calcium ion interacted with 5-FU loaded MCM-41-PAA matrix (Ca@MCM-41-PAA_5-FU), which was due to the complexation between the calcium ions and carboxyl

Preprints (www.preprints.org) | NOT PEER-REVIEWED | Posted: 2 August 2022 doi:10.20944/preprints202208.0066.v1

groups in the polymeric layer. The interactions in the polymeric layer were dissociated under acidic conditions.

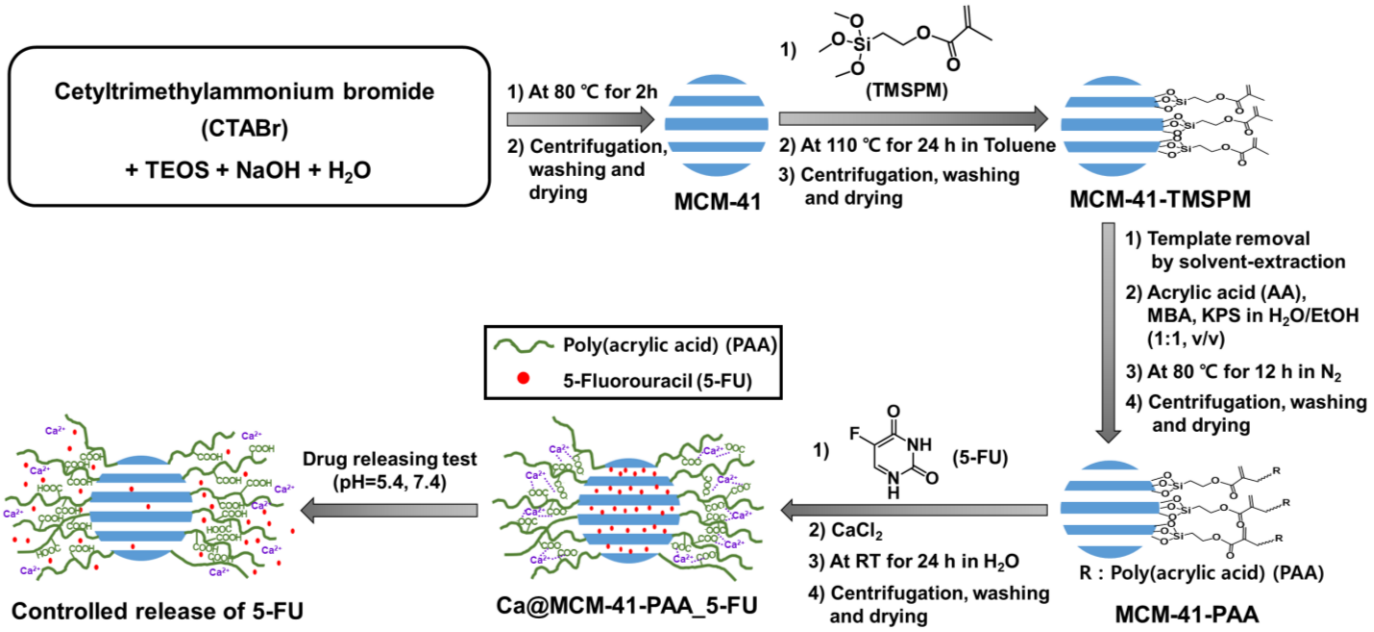

Scheme 1. An illustration for the preparation of Ca@MCM-41-PAA_5-FU and the releasing behavior of drug molecules in pH stimulus.

3.2. Characterization of MCM-41 and functionalized MCM-41

3.2.1. Scanning electron microscopy (SEM) and Transmission electron microscopy (TEM)

Figure 1 shows SEM images of (a, e) MCM-41, (b, f) MCM-41-TMSPM, (c, g) MCM-41-PAA and (d, h) Ca@MCM-41-PAA_5-FU. The images (Figure 1a and 1e) of the pristine MCM-41 exhibited a homogenous spherical morphology of particles with an average size of around 140 nm. After the functionalization of polyacrylic acid (PAA) on the surface (Figure 1c and 1g), the nanoparticles maintained their morphological integrity. The surface of the nanoparticles looks uneven which is presumed to be due to the grafting of polyacrylic acids. After the incorporation of calcium ions into the MCM-41-PAA (Figure 1d and 1h), the complexation of carboxyl functional groups and calcium ions also made the surface of the particle roughen.

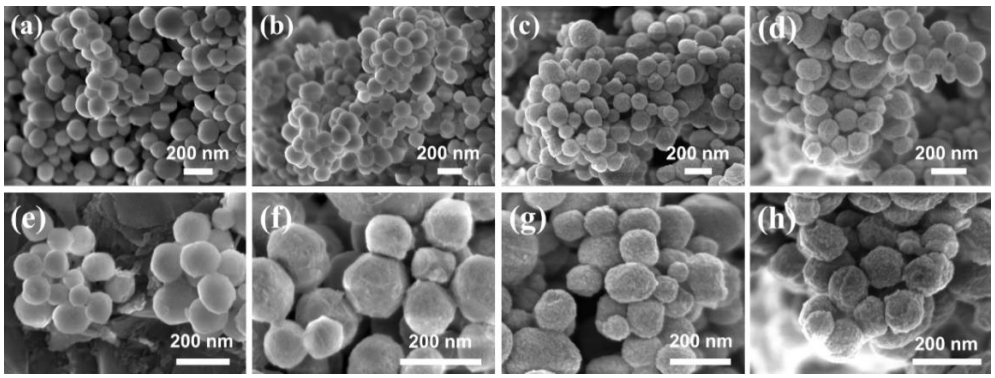

Figure 1. SEM images of (a, b) MCM-41, (c, d) MCM-41-TMSPM, (e, f) MCM-41-PAA, (g, h) Ca@MCM-41-PAA_5-FU.

Figure 2 shows TEM images of samples (2a-2d). All the modified and unmodified MCM-41 have well-organized periodic hexagonal mesopore arrays and present channel structures with parallel stripes. It proves that the ordered 2D hexagonal mesostructure was obtained in this work [52]. After the polymerization of PAA (Figure 2c), some

Preprints (www.preprints.org) | NOT PEER-REVIEWED | Posted: 2 August 2022 doi:10.20944/preprints202208.0066.v1

grafting of the polymer can be seen on the surface of MCM-41. In the TEM images of the Figure 2d, one can observe the coating of polymeric layers on the surface but no significant difference from the prior step's image (Figure 2c). The existence of calcium ions by the incorporation with carboxylate functional groups can be measured by the method of EDS mapping, which will be mentioned later. The structure without loss of well-arranged mesopore arrays in a long range after modification steps is preferred for loading guest molecules (Figure 2c and 2d) [53].

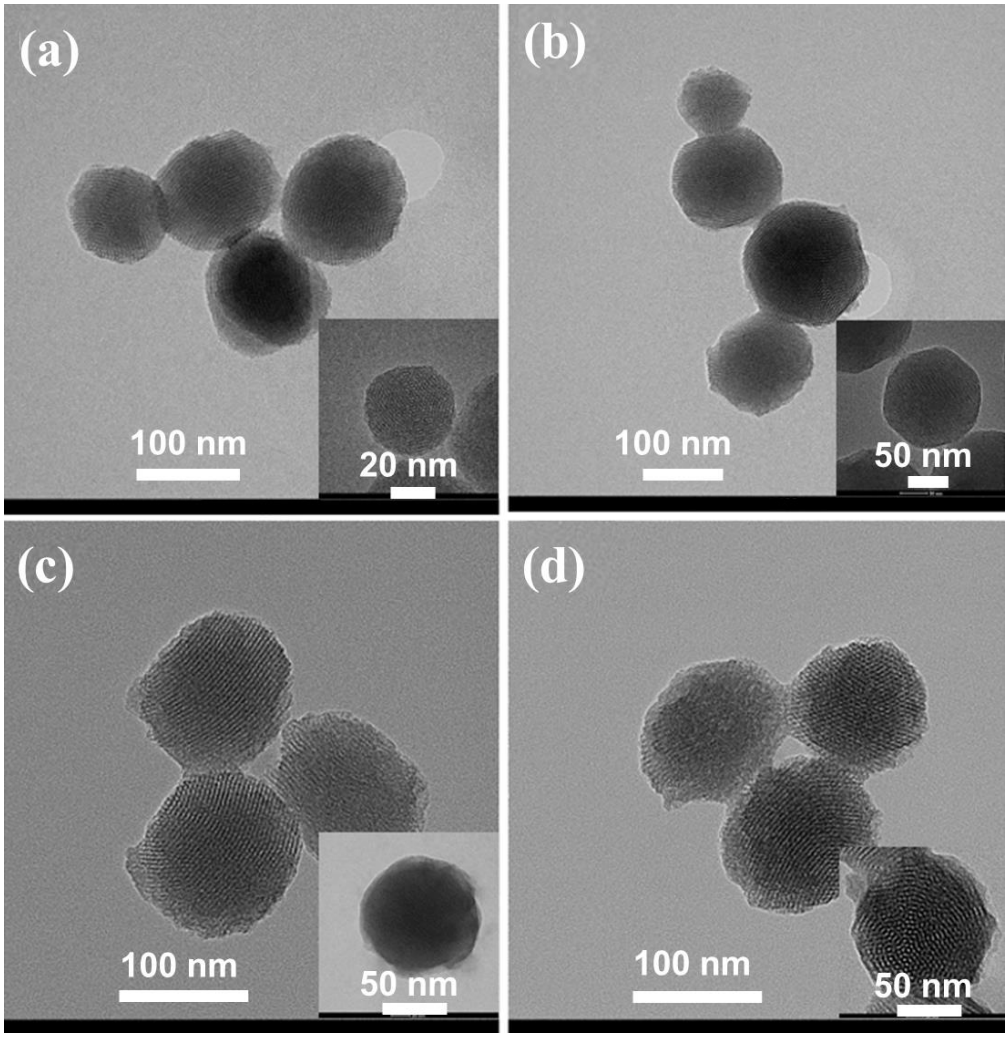

Figure 2. TEM images of (a) MCM-41, (b) MCM-41-TMSPM, (c) MCM-41-PAA, and (d) Ca@MCM-41-PAA_5-FU.

3.2.2. Elemental analysis

Figure 3 shows FE-TEM image (a), EDS mapping (b - g) and spectrum (i) of Ca@MCM-41-PAA_5-FU. The element Ca was observed with uniformly dispersed on the MCM-41-PAA nanoparticles (Figure 3h). Furthermore, the encapsulation of 5-FU can be proved by the presence of elements N and F in the nanostructure which comes from the component of 5-FU molecule (Figure 3c and 3d.). Other elements such as Si, O and C also can be confirmed. Especially, distinct dispersion of C elements around the sphere nanoparticle indicates PAA polymer coating was synthesized successfully. In addition, EDS spectra of Ca@MCM-41_5-FU demonstrate the weight percentage of Ca (0.73 wt%), N (1.94 wt%) and F (0.53 wt%) in the polymer functionalized MCM-41 nanocarrier.

Preprints (www.preprints.org) | NOT PEER-REVIEWED | Posted: 2 August 2022 doi:10.20944/preprints202208.0066.v1

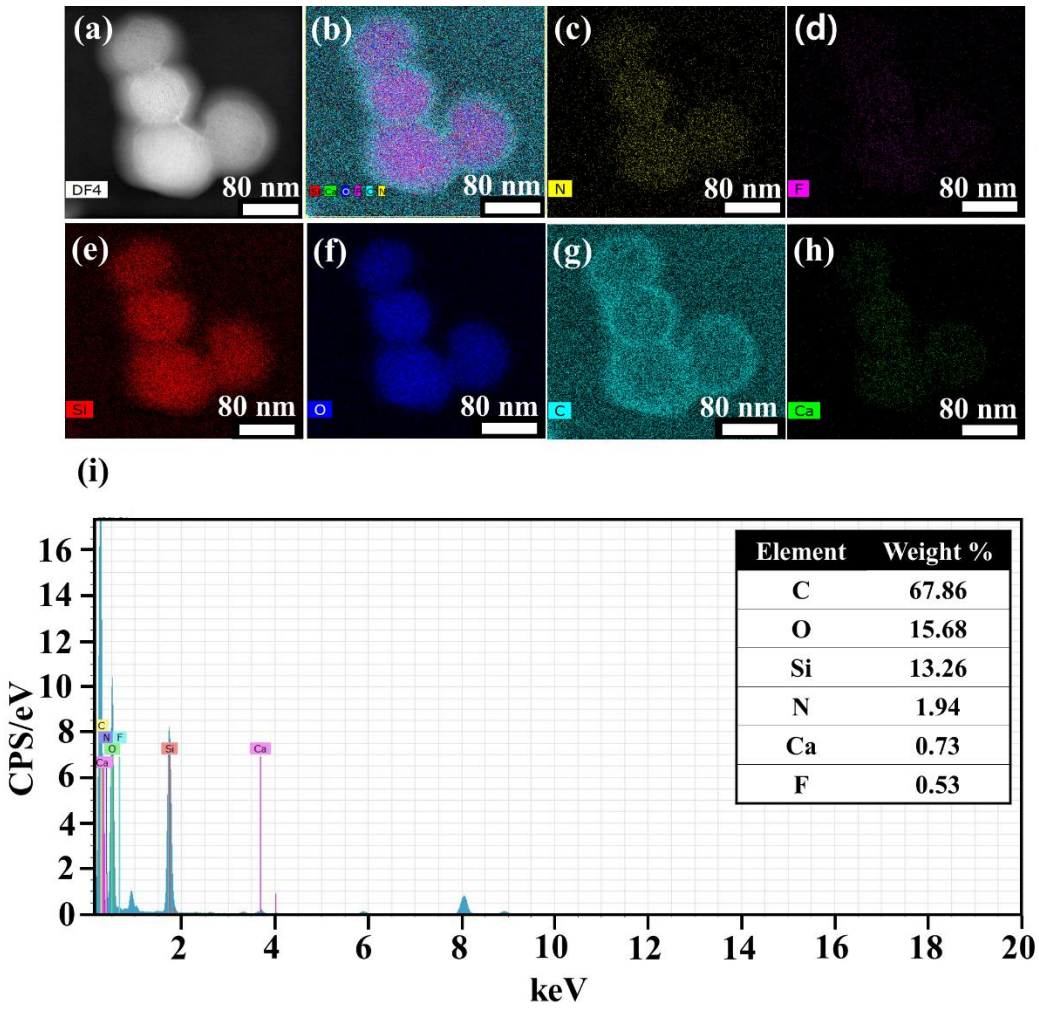

Figure 3. FE-TEM image (a), EDS mapping (b - g) and spectra (i) of Ca@MCM-41-PAA_5-FU.

3.2.3. X-ray diffraction (XRD)

Low-angle X-ray diffraction (LXRD) patterns of MCM-41, MCM-41-TMSPM, MCM-41-PAA, and Ca@MCM-41-PAA_5-FU are shown in Figure 4. MCM-41 presents intense reflections of d-spacing (100) and three additional peaks with low intensities at (110), (200) and (210), which are corresponding to the value of 2θ = 2.1°, 3.8°, 4.4°, and 5.7°, respectively (Figure 4a). These peaks can indicate the organized structure of samples associated with a p6mm hexagonal symmetry of the ordered MCM-41-type materials [54]. As a modification of TMSPM (Figure 4b) and functionalization of PAA (Figure 4c) proceeded, the intensities of d-spacing (110), (200) and (210) were successively decreased, which can be the proof of successful proceeding of the synthesis procedure without loss of mesoporous structural ordering. Also, broadening and slight shifts to the higher angle of d-spacing (100) and (200) occurred due to the functionalization of PAA on the mesopoprous silica [55]. The incorporation of 5-FU into the Ca@MCM-41-PAA_5-FU can be established by the significantly decreased intensity of LXRD peaks at d-spacing (100), (110) and (200) (Figure 4d). The wide-angle X-ray diffraction (WXRD) pattern of Ca@MCM-41-PAA_5-FU (Figure 5d) compensates for this fact. The WXRD patterns were measured to check up whether the crystalline phase of 5-FU molecules was shown on the surface of the pristine MCM-41 and the functionalized mesoporous silica nanoparticles. On the WXRD pattern of 5-FU, a characteristic strong peak at 2θ = 28° is observed (Figure 5a) [56]. In the case of 5-FU loaded nanoparticles such as MCM-41_5-FU, MCM-41-PAA_5-FU and Ca@MCM-41-PAA_5-FU, broad diffraction peak at 2θ values between 17° and 36° with very low intensities, which are typical for the amorphous state of silica structure [55] (Figure 5b-5d). These patterns without specific peaks of 5-FU imply that the total incorporation of 5-FU

Preprints (www.preprints.org) | NOT PEER-REVIEWED | Posted: 2 August 2022 doi:10.20944/preprints202208.0066.v1

into the mesopores was well proceeded with no existence of 5-FU cluster on the outer surface.

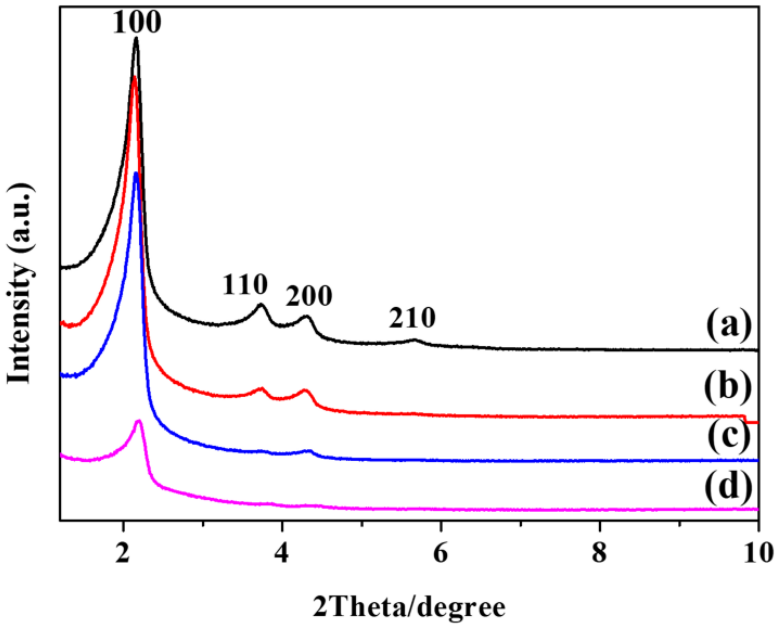

Figure 4. Low-angle XRD patterns of (a) MCM-41, (b) MCM-41-TMSPM, (c) MCM-41-PAA, and (d) Ca@MCM-41-PAA_5-FU.

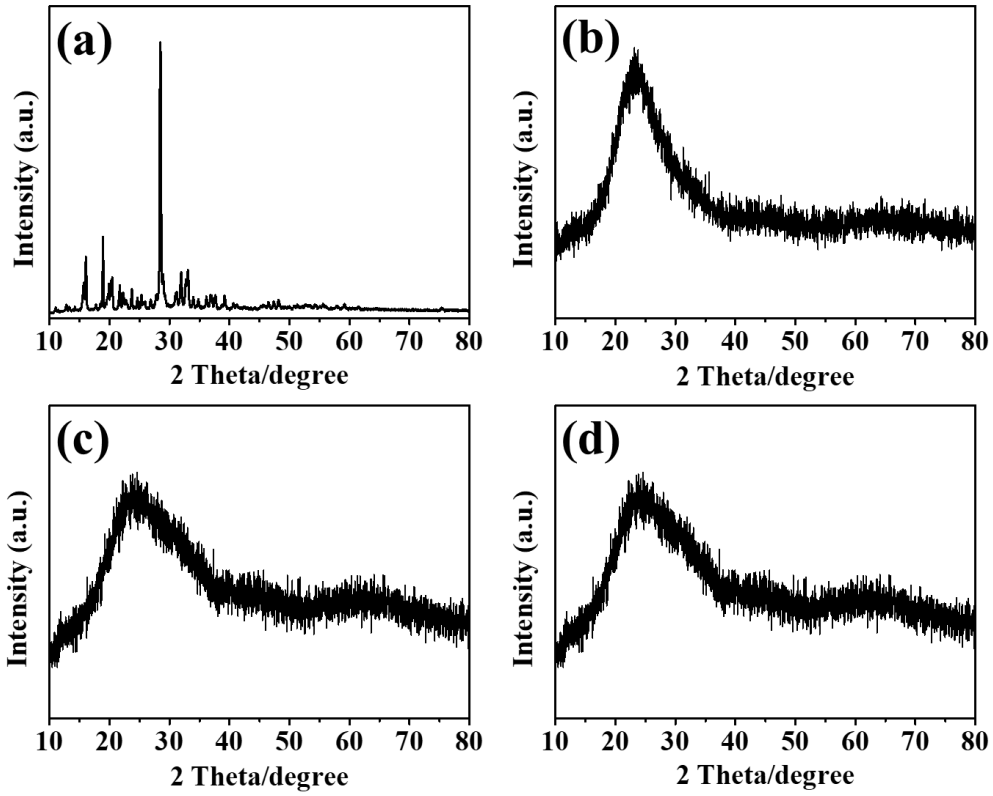

Figure 5. Wide-angle XRD patterns of (a) 5-FU, (b) MCM-41_5-FU, (c) MCM-41-PAA_5-FU, and (d) Ca@MCM-41-PAA_5-FU.

3.2.4. Thermogravimetric (TG) analysis

By the measurement of TGA analysis (Figure 6), one can observe the extent of functionalization of each proceeding steps and loading of guest molecules (5-FU) can be observed in mesoporous nanoparticle samples. The weight percentage after heating up to

Preprints (www.preprints.org) | NOT PEER-REVIEWED | Posted: 2 August 2022 doi:10.20944/preprints202208.0066.v1

800 °C with a rate of 10 °Cmin^{-1} in a nitrogen atmosphere of MCM-41, MCM-41-TMSPM, MCM-41-PAA, and Ca@MCM-41-PAA_5-FU were 89.9%, 80.1, 70.1%, and 65.2%, respectively. The initial weight loss under 200 °C is caused by thermo-desorption of physisorbed water or residual solvents [50]. A decrease of weight from 200 to 800 °C was assigned to the loss of organic functional groups on the mesopore walls. During this process, water molecules may also form through the silanol condensation in the pore walls [57]. In the case of MCM-41 (Figure 6a), the degradation of the remained CTAB surfactant (from 180 to 340 °C) and the condensation of silanol groups (Si-OH) (up to 800 °C) in the frameworks can be occurred resulting in 10.1% weight loss [58]. Likewise, the total weight loss of the samples was 19.9% for MCM-41-TMSPM (Figure 6b) and 29.9% for the MCM-41-PAA (Figure 6c) due to the decomposition of TMSPM and PAA organic functional groups, respectively. Also, 34.8% weight loss of Ca@MCM-41-PAA_5-FU can be proof of loading of 5-FU drugs inside mesopores (Figure 6d). The increase of weight loss implies that a much higher extent of functionalization with the organic groups or loading of 5-FU was proceeded at this time in steps [59].

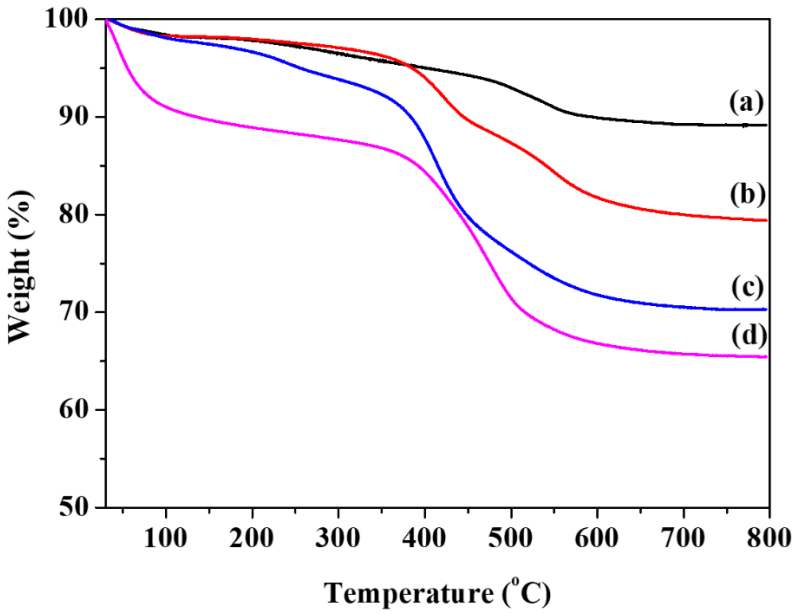

Figure 6. TGA curves of (a) MCM-41, (b) MCM-41-TMSPM, (c) MCM-41-PAA, and (d) Ca@MCM-41-PAA_5-FU.

3.2.5. Fourier transform infrared (FTIR) spectroscopy

Figure 7 shows FTIR spectra which make it possible to evaluate the surface functionalization of mesoporous silica nanoparticles. In the FTIR spectrum of MCM-41 as shown in Figure 7a, the intense peak at 1082 cm^{-1} was appeared as Si–O–Si antisymmetric stretching vibration. Besides this peak, the peaks at 959, 797, and 459 cm^{-1} ascribed to the bending vibration of the Si–OH, symmetric stretching vibration of the Si–O–Si and the stretching vibration of Si–O, respectively [60]. All these peaks are characteristic adsorption peaks of mesoporous silica (SiO_2). The broad peaks at 3419 cm^{-1} and absorption peaks at 1629 cm^{-1} in this sample appeared due to the OH stretching and H–O–H bending vibration adsorbed water. In the case of MCM-41-TMSPM (Figure 7b), additional peaks at 2953 and 2892 cm^{-1} correspond to the asymmetric and symmetric C–H stretching which can be proof of successful modification of TMSPM on the surface. Likewise, adsorption peaks of ester C=O stretching and C=C stretching vibration of TMSPM molecule structure are measured at 1708 and 1635 cm^{-1}, respectively [61]. After functionalization of PAA (Figure 7c), one can observe the carbonyl C=O stretching vibration peak of carboxylic acid at 1719 cm^{-1} which has a more obvious intensity than the C=O stretching adsorption peak of TMSPM. In addition, the peak at 1402 cm^{-1} was obtained due to the symmetric O–C–O stretching vibration of the carboxyl groups [62]. In the spectrum of Ca@MCM-41-PAA_5-FU (Figure 7d),

Preprints (www.preprints.org) | NOT PEER-REVIEWED | Posted: 2 August 2022 doi:10.20944/preprints202208.0066.v1

O–C–O stretching vibration peaks of carboxylate groups were observed at 1568 and 1412 cm^{-1}. Typical O–C–O stretching adsorption peaks appear at the wavelength near 1578 and 1402 cm^{-1}. When Ca^{2+} ions existed, the pair of bands was observed to shift about 10 cm^{-1} respectively. Therefore, changes in the position of the carboxylate group's adsorption peaks display that the polymer-metal ion complex on the surface of MCM-41 was formed by the interaction between carboxylate groups and the metal ions [63].

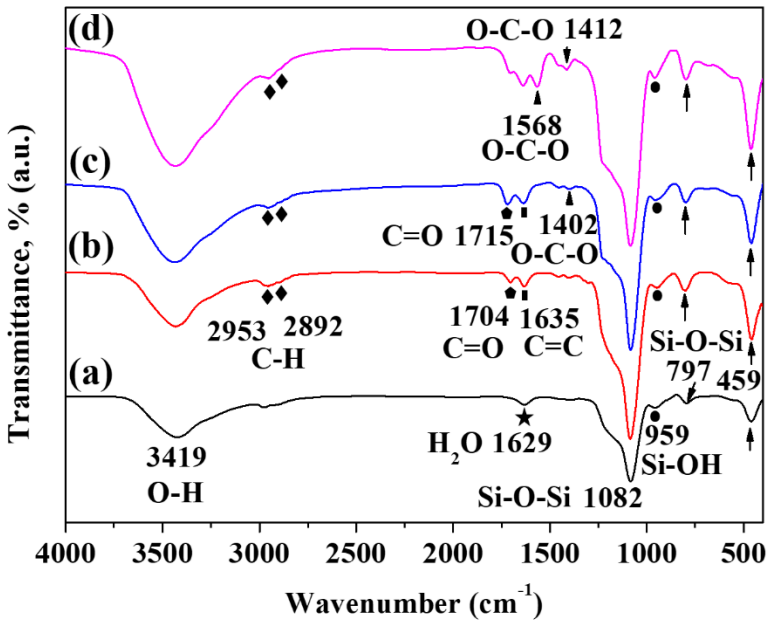

Figure 7. FT-IR spectra of (a) MCM-41, (b) MCM-41-TMSPM, (c) MCM-41-PAA, and (d) Ca@MCM-41-PAA_5-FU.

3.2.6. N_2 adsorption-desorption isotherms and pore size distributions

N_2 adsorption-desorption isotherms (Figure 8A) and pore size distributions (Figure 8B) of MCM-41, MCM-41-PAA and Ca@MCM-41-PAA_5-FU are shown in Figure 8. Table 1 lists the surface area, pore volume and pore size of MCM-41, MCM-41-PAA and Ca@MCM-41-PAA_5-FU. Among various kinds of isotherms, Type IV was gained because of the structure of the mesopore [64]. Type IV isotherms are appeared by capillary condensation and it has a hysteresis loop because of the difference between monolayer-multilayer adsorption and desorption characteristics [64]. In the case of MCM-41, it has a high surface area (900 m^2g^{-1}), large pore volume (0.85 cm^3g^{-1}) and pore size (2.7 nm), which is sufficient to be used as the functionalized nanocarrier of guest molecules. After polymerization of acrylic acid, the surface area, pore volume and pore size were decreased due to the presence of functional groups of PAA that partly block the adsorption of nitrogen molecules on the surface. The decrease of these parameter values indicates the polymerization of acrylic acid proceeded well and the PAA groups covered the wall of nanoparticles. Also, the decline of surface area, pore volume and pore size of Ca@MCM-41-PAA_5-FU compared to MCM-41-PAA shows that the loading of 5-FU drugs and calcium ions occurred in the mesopores. And it appears Type III isotherm characteristics on Ca@MCM-41-PAA_5-FU which can be attributed to partial loading of 5-FU drugs and some of the calcium ions in mesopores that hinder steep capillary condensation [65]. Meanwhile, for the pore size of Ca@MCM-41-PAA_5-FU, it was too low value to measure (< 2.0 nm).

Preprints (www.preprints.org) | NOT PEER-REVIEWED | Posted: 2 August 2022 doi:10.20944/preprints202208.0066.v1

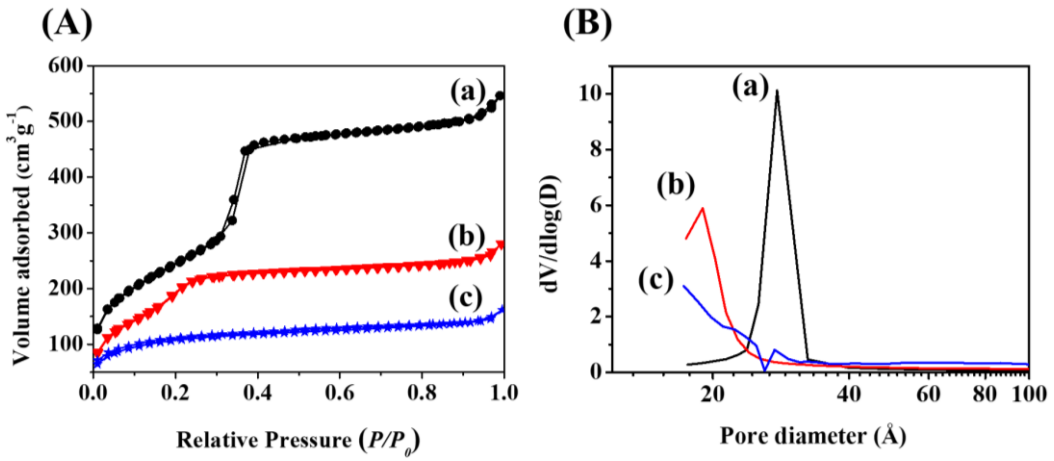

Figure 8. N_2 adsorption-desorption isotherms (A) and pore size distributions (B) of (a) MCM-41, (b) MCM-41-PAA and (c) Ca@MCM-41-PAA_5-FU.

Table 1. BET surface area, pore volume and pore size of MCM-41, MCM-41-PAA and Ca@MCM-41-PAA_5-FU.

Samples	BET Surface area (m^2g^{-1})	Pore volume (cm^3g^{-1})	Pore size (nm)
MCM-41	900	0.85	2.7
MCM-41-PAA	753	0.43	1.9
Ca@MCM-41-PAA_5-FU	358	0.25	-

3.2.7. Zeta potential

As shown in Table 2, zeta potential measurements were carried out to figure out the surface charge of MCM-41, MCM-41-TMSPM, MCM-41-PAA, MCM-41_5-FU, MCM-41-PAA_5-FU, and Ca@MCM-41-PAA_5-FU in aqueous suspensions. In the case of MCM-41, the massive number of silanol groups on the surface proceed to the negative zeta potential value of -18.3 mV assuring that the negative charges ($Si\text{-}O^-$) were generated from deprotonated silanol groups [65]. After modification of TMSPM, the zeta potential value of MCM-41-TMSPM is shifted to -0.135 mV due to the terminal alkenyl groups which have relatively neutral charges than that of silanol groups [67]. Subsequent functionalization of PAA led zeta potential values to decrease up to -51 mV, as carboxyl groups (−COOH) are deprotonated as negatively charged carboxylate groups ($-COO^-$). This obvious change of zeta potential value verifies the existence of much amount of carboxylic acid groups on the nanoparticle surface which are positioned by functionalization of PAA [68]. Likewise, the zeta potential was measured after loading 5-FU into the MCM-41, MCM-41-PAA and calcium incorporated MCM-41 samples. In the case of MCM-41_5-FU, the early burst of 5-FU in an aqueous solution may affect the surface charges of MCM-41 by forming hydrogen bonds between silanol groups and 5-FU which has N and F elements in molecule structure [69]. By this reason, the zeta potential value changes to 0.132 mV. Otherwise, the value of 5-FU loaded MCM-41-PAA (MCM-41-PAA_5-FU) has no big difference from that of MCM-41-PAA. It might be less affected by the release of drugs which is less amount compared to the release of MCM-41_5-FU. Also, the massive amount of carboxyl acid groups in PAA chains can compensate for the variable factor-changing zeta potential of the nanoparticle surface. The sample loaded with both 5-FU and calcium ion (Ca@MCM-41-PAA_5-FU) has a zeta potential value of 0.0108 mV. This zeta potential value convinces that the interaction between carboxyl groups and calcium ions was formed, resulting in a

Preprints (www.preprints.org) | NOT PEER-REVIEWED | Posted: 2 August 2022 doi:10.20944/preprints202208.0066.v1

negatively charged surface of MCM-41-PAA that would be neutralized in aqueous suspension.

Table 2. Zeta potential values of MCM-41, MCM-41-TMSPM, MCM-41-PAA, MCM-41_5-FU, MCM-41-PAA_5-FU, and Ca@MCM-41-PAA_5-FU.

Sample	Zeta Potential (mV)
MCM-41	-18.3
MCM-41-TMSPM	-0.135
MCM-41-PAA	-51
MCM-41_5-FU	0.132
MCM-41-PAA_5-FU	-57.2
Ca@MCM-41-PAA_5-FU	0.0108

3.2.8. Dynamic light scattering (DLS)

The hydrodynamic diameters of MCM-41 (Figure 9Aa) and MCM-41-PAA (Figure 9Ab) can be obtained in aqueous solutions by DLS analysis (Figure 9A). the particle diameter of MCM-41 and MCM-41-PAA was 267.4 and 335.0 nm, respectively. These sizes are much bigger than that are measured by SEM because of the existence of nonuniformly dispersed particles and the formation of a hydrated layer in water [70]. The increase in particle size of MCM-41-PAA compared to MCM-41 was made by the existence of hydrophilic PAA chains on the surface of MCM-41 and the robustness of adhesion between MCM-41-PAA nanoparticles than MCM-41 [71]. Also, the particle size of Ca@MCM-41-PAA was observed at different pH environments in PBS buffer to compare the pH-responsive behavior of the polymer-metal ion complex layer (Figure 9B). The hydrodynamic diameter was 394.0 nm at pH 5.4 (Figure 9Ba) and 349.7 nm at pH 7.4 (Figure 9Bb), respectively. The decrease of diameter at higher pH (7.4) implies that the contraction of polymer chains occurred by the interaction with calcium ions.

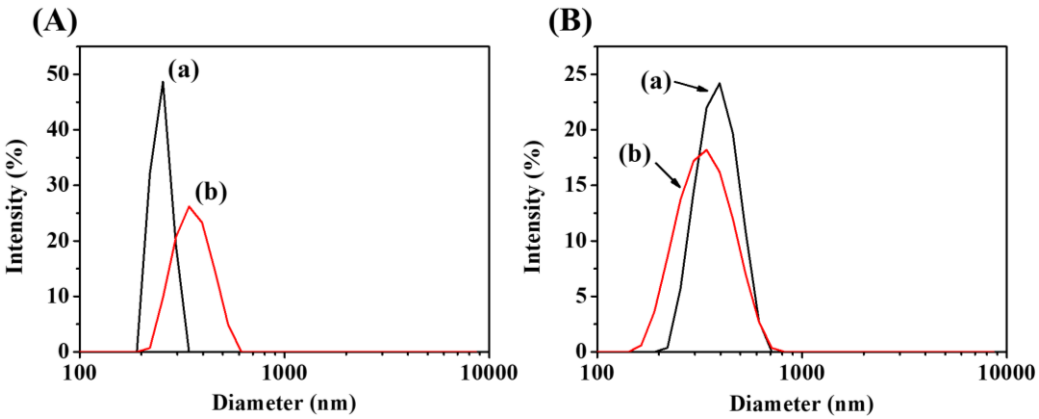

Figure 9. DLS curves of (A), (a) MCM-41 and (b) MCM-41-PAA; (B), Ca@MCM-41-PAA_5-FU with different pH environment of (a) pH 5.4 and (b) 7.4.

3.2.9. Drug releasing test

Figure 10 shows the in-vitro 5-FU releasing profiles of 5-FU loaded MCM-41 (A) MCM-41_5-FU), 5-FU loaded MCM-41PAA ((B) MCM-41-PAA_5-FU), and 5-FU loaded MCM-41-PAA encapsulated by polymer-calcium ion complex ((C) Ca@MCM-41-PAA_5-FU) at (a) pH 5.4 and (b) 7.4 for 72 h, respectively. As shown in Figure 10A, the burst release of 5-FU was observed and the total release amount was as high as close to 90~95%.

Preprints (www.preprints.org) | NOT PEER-REVIEWED | Posted: 2 August 2022 doi:10.20944/preprints202208.0066.v1

This result is attributed to the dissociation of physically adsorbed 5-FU with silanol groups on the surface of MCM-41. Meanwhile, it shows a higher release amount at a pH 5.4 environment than that of pH 7.4 due to the partial protonation of 5-FU and silanol groups on the surface of MCM-41 that causes electrostatic repulsion of drug molecules under lower pH condition. At neutral pH condition, both hydrophilic 5-FU and silanol groups made a hydrophilic-hydrophilic interactions and hydrogen bonding could be formed so that the release rate of 5-FU drugs could be slower [72].

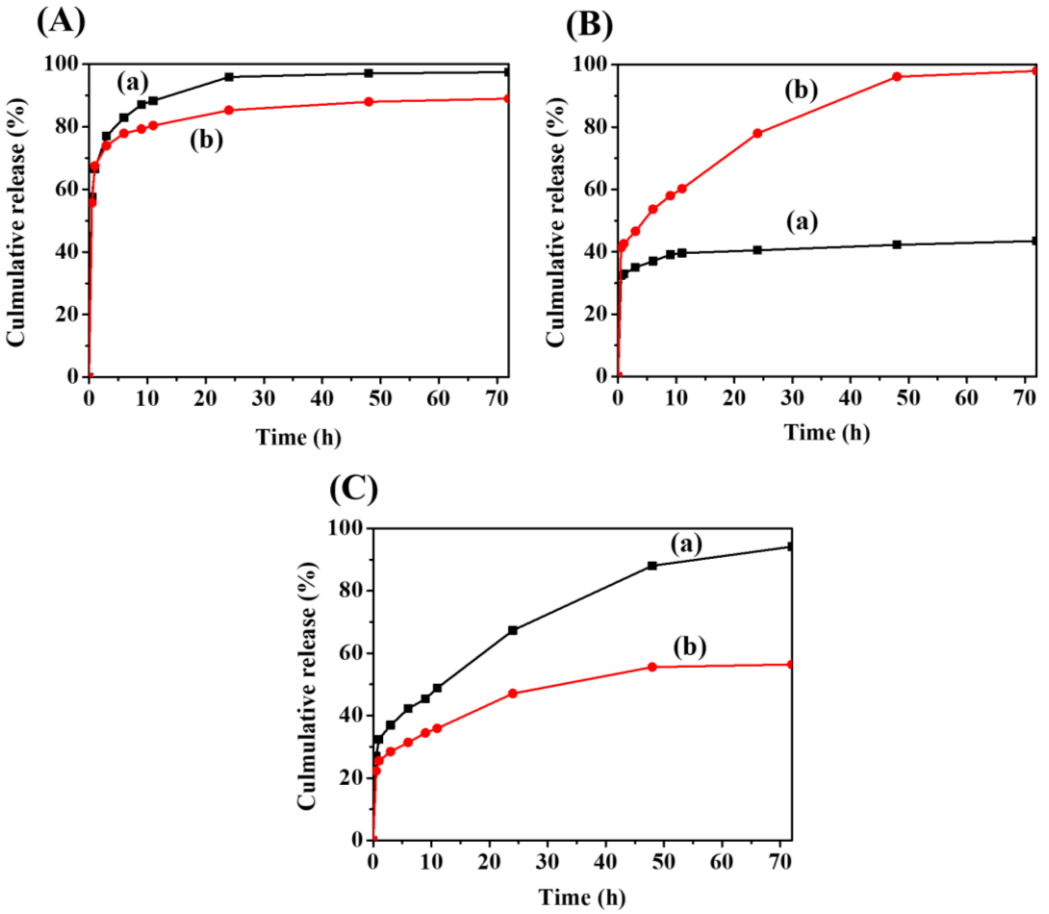

Figure 10. In-vitro 5-FU release profiles of (A) MCM-41_5-FU, (B) MCM-41-PAA_5-FU, and (C) Ca@ MCM-41-PAA_5-FU with different pH environment of (a) pH 5.4 and (b) 7.4.

In the case of 5-FU loaded MCM-41-PAA (MCM-41-PAA_5-FU) (Figure 10B), it shows a significantly high total release amount in pH 7.4 (96.6%) compared to pH 5.4 (42.5%). At a neutral pH environment, carboxylic acid groups can alter their ionization/deprotonation behavior depending on the pH environment. Most of the carbonyl groups of polyacrylic acid (pKa = 4.8) are negatively charged at pH 7.4 which makes electrostatic repulsion between polymer chains. Also, its high solubility results in PAA chains' swelling behavior. the opened pore state caused by this behavior of polymers made 5-FU yielding to moving to the exit of pores and the release in solutions. Note that there is no significant interaction between 5-FU (pKa = 8.2) and carboxyl groups [72]. In contrast, in a pH 5.5 environment, contraction of PAA chains by protonation could block the pore exit so the release of 5-FU would be hindered [71].

Compared to the result of Figure 10B, in Figure 10C, the tendency of drug release amount was changed. The total release amount in pH 5.4 and pH 7.4 was 93.7% and 54.1%, respectively. In a neutral environment (pH 7.4), the carboxylate groups with negative charges could form COO^{-}–Ca^{2+} electrostatic interaction. This ionic bond makes a polymer-metal ion complex layer around MCM-41 nanoparticles, so the release of 5-FU would be obstructed. At pH 7.4, however, some of the 5-FU molecules can be deprotonated [73],

Preprints (www.preprints.org) | NOT PEER-REVIEWED | Posted: 2 August 2022 doi:10.20944/preprints202208.0066.v1

then the interaction between 5-FU and calcium ion could be formed that can break the COO^{-}–Ca^{2+} interaction. This disassociation of polymer-metal ion bond could arise leakage of 5-FU drugs contained in mesopores. At pH 5.4, the interacted polymer-calcium ion layer was disbanded and the drug release amount increased. The protonation of carboxyl groups at comparably low pH leads to withdraw electrostatic interaction between COO^{-} and Ca^{2+}. This disruption of the polymer-metal ion layer led to the obvious release of 5-FU drugs into the solution. Also, Cl^{-} ion in PBS buffer could replace the carboxylate groups to destroy the ionic interaction between COO^{-} and Ca^{2+} [74]. By these results, the Ca^{2+} interacting polymeric layer could act as a pH-selective drug release barrier and inhibit burst release in a normal physiological environment.

In a mildly acidic environment (pH 5.4), the polymeric gate of Ca@MCM-41-PAA_5-FU helped to proceed controlled release of 5-FU and Ca^{2+} ions. Meanwhile, at pH 7.4, the gate of nanoparticles remained mostly closed and the drugs were stored because of the maintenance of the calcium ion-polymeric layer. If this nanocomplex got into the cancer cell by endocytosis, the interaction between calcium ion and polymer would be destroyed in a low pH cytoplasm system with higher concentration on Cl^{-}, which can raise the higher release of 5-FU drugs. Also, calcium ion can enhance the apoptosis of cancer cell too [75]. Consequently, we can predict that this gating mechanism has a possibility to be applied to various medical treatments by its specific pH responsiveness for 5-FU release. Furthermore, this stimuli-responsive property of the synthesized material shows potential as an effective delivery system for many applications in industry.

To confirm the release mechanism, the drug release results were fitted to the following Korsmeyer-Peppas equation [71]

$$\frac{M_t}{M_\infty} = k_p t^n$$

In this equation, M_t/M_∞ is a fraction of the drug release of 5-FU at time t, k_p is the rate constant, and n is the release exponent. By using the least-squares procedure, the values of n and k were estimated for all formulations as shown in Table 3. The n value was used to characterize the release mechanism of the samples (MCM-41_5-FU, MCM-41-PAA_5-FU and Ca@MCM-41-PAA_5-FU). For n = 0.5, the drug diffuses according to Fickian type diffusion. If $0.5 < n < 1$, anomalous or non-Fickian drug diffusion works. In the case of n = 1, case II transport of drug kinetics occurs. In this work, the n values were under $n < 0.5$ (between 0.09 and 0.3), assuring a Fickian diffusion trend, which approves non-swellable property of MCM-41 nanostructure. The in vitro release results imply that these nanocarriers can be applied for the delivery of anticancer drugs.

Table 3. In vitro release data of MCM-41, MCM-41-PAA_5-FU and Ca@MCM-41-PAA_5-FU for various formulations.

Sample	pH 5.4			pH 7.4		
	n	k	r	n	k	r
MCM-41_5-FU	0.097	0.695	0.9852	0.079	0.736	0.9876
MCM-41-PAA_5-FU	0.067	0.731	0.9894	0.22	0.397	0.9727
Ca@MCM-41-PAA_5-FU	0.30	0.282	0.9769	0.22	0.399	0.9715

4. Conclusions

 doi:10.20944/preprints202208.0066.v1

Polyacrylic acid-functionalized MCM-41 was synthesized by free radical polymerization by using acrylic acid monomer, TMSPM as a linker material, CTABr as structure-directing agents and TEOS as a silica precursor. The successful functionalization of PAA on the surface of MCM-41 by the analysis of various characterization measurements. After that, the drug release was investigated was confirmed using 5-FU as a model anticancer drug with incorporating calcium ions. As a result, the carboxyl group of outer the surface of nanoparticles ionically incorporated with calcium ions acted as a gate of the pores, which showed remarkable pH-responsive activity by the result of 5-FU release profiles in pH 5.4 and 7.4. Disassociation of ionic bond of calcium ion-polymeric layer in the functionalized MCM-41 (Ca@MCM-41-PAA_5-FU) helped to proceed pH-stimulus selective release of 5-FU and calcium ions at pH 5.4. The total drug release amount was roughly two times higher at pH 5.4 than under a neutral environment (pH 7.4). The highly released 5-FU can act as a cancer treatment agent and calcium ions can induce apoptosis of cancer cells in the body. Meanwhile, at pH 7.4, the gate of nanoparticles remained closed and the drug release rate is not high. By these results, it is predicted that this gating mechanism has the possibility to be applied to various medical treatments by its specific pH responsiveness. Also, the stimuli-responsive property of synthesized material shows potential as an effective delivery system for other applications.

Author Contributions: Conceptualization, J.K. and S.S.P.; methodology, J.K. and S.S.P.; software, J.K. and S.S.P.; validation, J.K., S.S.P. and C.-S.H.; formal analysis, J.K.; investigation, J.K.; resources, C.-S.H.; data curation, J.K.; writing—original draft preparation, J.K.; writing—review and editing, S.S.P. and C.-S.H.; visualization, J.K. and S.S.P.; supervision, C.-S.H.; project administration, S.S.P. and C.-S.H.; funding acquisition, S.S.P. and C.-S.H. All authors have read and agreed to the published version of the manuscript.

Funding: The work was supported by the National Research Foundation of Korea (NRF) Grant funded by the Ministry of Science and ICT, Korea (2021R1I1A3060098, NRF-2021R1I1A3059777 and Brain Korea 21 Plus Program (4199990414196)) and by the Korea Institute for Advancement of Technology funded by the Ministry of Trade, Industry and Energy (P0017531).

Institutional Review Board Statement: Not applicable.

Informed Consent Statement: Not applicable.

Data Availability Statement: Not applicable.

Conflicts of Interest: The authors declare no conflict of interest.

References

1. Rehkopf, J.D.; Barbat, S.D.; Goldman, N.M.; Samus, M.A.; Gold, H. Environmentally responsive material to address human-system interaction in the automotive cockpit. *Smart Mater. Struct.: Industrial and Commercial Applications of Smart Structures Technologies* **2001**, *4332*, 217-224.
2. Basheer, A.A. Advances in the smart materials applications in the aerospace industries. *Aircr. Eng. Aerosp. Technol.* **2020**, *92*(7), 1027-1035.
3. Liu, Y.; Du, H.; Liu, L.; Leng, J. Shape memory polymers and their composites in aerospace applications: a review. *Smart Mater. Struct.* **2014**, *23*(2), 023001.
4. Nie, J.; Chen, X.; Wang, Z.L. Electrically responsive materials and devices directly driven by the high voltage of triboelectric nanogenerators. *Adv. Funct. Mater.* **2019**, *29*(41), 1806351.
5. Zhang, J. Switchable and responsive surfaces and materials for biomedical applications. Elsevier, Cambridge, UK, **2014**; pp. 3-43.
6. Gamerith, C.; Luschnig, D.; Ortner, A.; Pietrzik, N.; Guse, J.; Burnet, M.; Haalboom, M.; Palen, J. V. D.; Heinzle, A.; Sigl, E.; Gübitz, G.M. pH-responsive materials for optical monitoring of wound status. *Sens. Actuators B Chem.* **2019**, *301*, 126966.
7. Caldorera-Moore, M.; Peppas, N.A. Micro-and nanotechnologies for intelligent and responsive biomaterial-based medical systems. *Adv. Drug Deliv. Rev.* **2009**, *61*(15), 1391-1401.
8. Zhang, P.; An, K.; Duan, X.; Xu, H.; Li, F.; Xu, F. Recent advances in siRNA delivery for cancer therapy using smart nanocarriers. *Drug Discov. Today*. **2018**, *23*(4), 900-911.
9. Hossen, S.; Hossain, M.K.; Basher, M.; Mia, M.; Rahman, M.; Uddin, M.J. Smart nanocarrier-based drug delivery systems for cancer therapy and toxicity studies: A review. *J. Adv. Res.* **2019**, *15*, 1-18.
10. Choi, K.Y.; Yoon, H.Y.; Kim, J.H.; Bae, S.M.; Park, R.W.; Kang, Y.M.; Kim, I.S.; Kwon, I.C.; Choi, K.; Jeong, S.Y.; Kim, K.; Park, J.H. Smart nanocarrier based on PEGylated hyaluronic acid for cancer therapy. *ACS Nano* **2011**, *5*(11), 8591-8599.

11. Kalaydina, R.-V.; Bajwa, K.; Qorri, B.; Decarlo, A.; Szewczuk, M.R. Recent advances in "smart" delivery systems for extended drug release in cancer therapy. *Int. J. Nanomedicine* **2018**, *13*, 4727-4745.
12. Chabner, B.A.; Roberts, T.G. Chemotherapy and the war on cancer. *Nat. Rev. Cancer* **2005**, *5*(1), 65-72.
13. Chari, R.V. Targeted cancer therapy: conferring specificity to cytotoxic drugs. *Acc. Chem. Res.* **2008**, *41*(1), 98-107.
14. Bagnyukova, T.V.; Serebriiskii, I.G.; Zhou, Y.; Hopper-Borge, E.A.; Golemis, E.A.; Astsaturov, I. Chemotherapy and signaling: How can targeted therapies supercharge cytotoxic agents?. *Cancer Biology & Therapy* **2010**, *10*(9), 839-853.
15. Kwon, S.; Singh, R.K.; Perez, R.A.; Neel, E.A.A.; Kim, H.-W.; Chrzanowski, W. Silica-based mesoporous nanoparticles for controlled drug delivery. *J. Tissue Eng.* **2013**, *4*, 2041731413503357.
16. Yang, P.; Gai, S.; Lin, J. Functionalized mesoporous silica materials for controlled drug delivery. *Chem. Soc. Rev.* **2012**, *41*(9), 3679-3698.
17. Slowing, I.I.; Vivero-Escoto, J.L.; Wu, C.-W.; Lin, V.S.-Y. Mesoporous silica nanoparticles as controlled release drug delivery and gene transfection carriers. *Adv. Drug Deliv. Rev.* **2008**, *60*(11), 1278-1288.
18. Theato, P.; Sumerlin, B.S.; O'Reilly, R.K.; Epps III, T.H. Stimuli responsive materials. *Chem. Soc. Rev.* **2013**, *42*(17), 7055-7056.
19. Guragain, S.; Bastakoti, B.P.; Malgras, V.; Nakashima, K.; Yamauchi, Y. Multi-stimuli-responsive polymeric materials. *Chem. Eur. J.* **2015**, *21*(38), 13164-13174.
20. Gago, S.; Zhang, Y.; Santos, A.M.; Kohler, K.; Kuhn, F.E.; Fernandes, J.A.; Pillinger, M.; Valente, A.A.; Santos, T.M.; Ribeiro-Claro, P.J.A.; Goncalves, I.S. Synthesis and characterization of a manganese (II) acetonitrile complex supported on functionalized MCM-41. *Microporous Mesoporous Mater.* **2004**, *76*(13), 131-136.
21. Jafarzadeh-Holagh, S.; Hashemi-Najafabadi, S.; Shaki, H.; Vasheghani-Farahani, E. Self-assembled and pH-sensitive mixed micelles as an intracellular doxorubicin delivery system. *J. Colloid Interface Sci.* **2018**, *523*, 179-190.
22. Lu, D.; Wen, X.; Liang, J.; Gu, Z.; Zhang, X.; Fan, Y. A pH-sensitive nano drug delivery system derived from pullulan/doxorubicin conjugate. *J. Biomed. Mater. Res. B Appl. Biomater.* **2009**, *89*(1), 177-183.
23. Cheng, Y.-J.; Qin, S.-Y.; Ma, Y.-H.; Chen, X.-S.; Zhang, A.-Q.; Zhang, X.-Z. Super-pH-sensitive mesoporous silica nanoparticle-based drug delivery system for effective combination cancer therapy. *ACS Biomater. Sci. Eng.* **2019**, *5*(4), 1878-1886.
24. Nik, A.B.; Zare, H.; Razavi, S.; Mohammadi, H.; Ahmadi, P.T.; Yazdani, N.; Bayandori, M.; Rabiee, N.; Mobarakeh, J.I. Smart drug delivery: Capping strategies for mesoporous silica nanoparticles. *Microporous and Mesoporous Mater.* **2020**, *299*, 110115.
25. Nandiyanto, A.B.D.; Kim, S.-G.; Iskandar, F.; Okuyama, K. Synthesis of spherical mesoporous silica nanoparticles with nanometer-size controllable pores and outer diameters. *Microporous and Mesoporous Mater.* **2009**, *120*(3), 447-453.
26. Petushkov, A.; Ndiege, N.; Salem, A.K.; Larsen, S.C. Toxicity of silica nanomaterials: zeolites, mesoporous silica, and amorphous silica nanoparticles. *J. Biochem. Mol. Toxicol.* **2010**, *4*, 223-266.
27. Oh, N.; Park, J.-H. Endocytosis and exocytosis of nanoparticles in mammalian cells. *Int. J. Nanomedicine* 2014, *9*(Suppl 1), 51-63.
28. Niedermayer, S.; Weiss, V.; Herrmann, A.; Schmidt, A.; Datz, S.; Müller, K.; Wagner, E.; Bein, T.; Bräuchle, C. Multifunctional polymer-capped mesoporous silica nanoparticles for pH-responsive targeted drug delivery. *Nanoscale* **2015**, *7*(17), 7953-7964.
29. Li, Z.; Yang, X.; Wu, L.; Chen, Z.; Lin, Y.; Xu, K.; Chen, G. Synthesis, characterization and biocompatibility of biodegradable elastomeric poly(ether-ester urethane)s based on poly (3-hydroxybutyrate-co-3-hydroxyhexanoate) and poly (ethylene glycol) via melting polymerization. *Biomater. Sci. Polym. Ed.* **2009**, *20*(9), 1179-1202.
30. Huang, Y.; Wang, D.; Zhu, X.; Yan, D.; Chen, R. Synthesis and therapeutic applications of biocompatible or biodegradable hyperbranched polymers. *Polym. Chem.* **2015**, *6*(15), 2794-2812.
31. Soliman, M.G.; Pelaz, B.; Parak, W.J.; Del Pino, P. Phase transfer and polymer coating methods toward improving the stability of metallic nanoparticles for biological applications. *Chem. Mater.* **2015**, *27*(3), 990-997.
32. Yang, Z.; Zeng, H.; Zhou, X.; Ji, H. Mechanism into selective oxidation of cinnamaldehyde using β-cyclodextrin polymer as phase-transfer catalyst. *Tetrahedron* **2012**, *68*(29), 5912-5919.
33. Solomon, M.; D'Souza, G.G.M. Approach to achieving sub-cellular targeting of bioactives using pharmaceutical. *In Intracellular Delivery: Fundamental Biomedical Technologies*, 2011th ed.; Prokop, A., Eds.; Springer: New York, USA, 2011; Volume 5, pp. 57-72.
34. Popescu, D.P.; Choo-Smith, L.; Flueraru, C.; Mao, Y.; Chang, S.; Disano, J.; Sherif, S.; Sowa, M.G. Optical coherence tomography: fundamental principles, instrumental designs and biomedical applications. *Biophys. Rev.* **2011**, *3*(3), 155-169.
35. Wan, X.; Zhang, G.; Liu, S. pH-disintegrable polyelectrolyte multilayer-coated mesoporous silica nanoparticles exhibiting triggered co-release of cisplatin and model drug molecules. *Macromol. Rapid Commun.* **2011**, *32*(14), 1082-1089.
36. Zhang, Y.M.; Liu, Y.H.; Liu, Y. Cyclodextrin-based multistimuli-responsive supramolecular assemblies and their biological functions. *Adv. Mater.* **2020**, *32*(3), 1806158.
37. Almeida, H.; Amaral, M.H.; Lobão, P. Temperature and pH stimuli-responsive polymers and their applications in controlled and selfregulated drug delivery. *J. Appl. Pharm. Sci.* **2012**, *2*(6), 1-10.
38. Lin, D.; Cheng, Q.; Jiang, Q.; Huang, Y.; Yang, Z.; Han, S.; Zhao, Y.; Guo, S.; Liang, Z.; Dong, A. Intracellular cleavable poly (2-dimethylaminoethyl methacrylate) functionalized mesoporous silica nanoparticles for efficient siRNA delivery in vitro and in vivo. *Nanoscale* **2013**, *5*(10), 4291-4301.
39. Soppimath, K.S.; Kulkarni, A.R.; Aminabhavi, T.M. Chemically modified polyacrylamide-g-guar gum-based crosslinked anionic microgels as pH-sensitive drug delivery systems: preparation and characterization. *J. Control Release* **2001**, *75*(3), 331-345.
40. Yang, P.; Li, D.; Jin, S.; Ding, J.; Guo, J.; Shi, W.; Wang, C. Stimuli-responsive biodegradable poly(methacrylic acid) based nanocapsules for ultrasound traced and triggered drug delivery system. *Biomaterials* **2014**, *35*(6), 2079-2088.
41. Chen, D.; Jiang, M.; Li, N.; Gu, H.; Xu, Q.; Ge, J.; Xia, X.; Lu, J. Modification of magnetic silica/iron oxide nanocomposites with fluorescent polymethacrylic acid for cancer targeting and drug delivery. *J. Mater. Chem.* **2010**, *20*(31), 6422-6429.

42. Chen, Q.; Li, S.; Feng, Z.; Wang, M.; Cai, C.; Wang, J.; Zhang, L. Poly(2-(diethylamino)ethyl methacrylate)-based, pH-responsive, copolymeric mixed micelles for targeting anticancer drug control release. *Int. J. Nanomedicine* **2017**, *12*, 6857-6870.
43. Bernkop-Schnürch, A.; Dünnhaupt, S. Chitosan-based drug delivery systems. *Eur. J. Pharm. Biopharm.* **2012**, *81*(3), 463-469.
44. Hu, L.; Sun, Y.; Wu, Y. Advances in chitosan-based drug delivery vehicles. *Nanoscale* **2013**, *5*(8), 3103-3111.
45. Mohammed, M.A.; Syeda, J.; Wasan, K.M.; Wasan, E.K. An overview of chitosan nanoparticles and its application in non-parenteral drug delivery. *Pharmaceutics* **2017**, *9*(4), 53.
46. Sahiner, N. A facile method for the preparation of poly (4-vinylpyridine) nanoparticles and their characterization. *Turk. J. Chem.* **2009**, *33*(1), 23-31.
47. Lu, H.; Yang, G.; Ran, F.; Gao, T.; Sun, C.; Zhao, Q.; Wang, S. Polymer-functionalized mesoporous carbon nanoparticles on overcoming multiple barriers and improving oral bioavailability of Probucol. *Carbohydr. Polym.* 2020, 229, 115508.
48. Singh, R.K.; Patel, K.D.; Leong, K.W.; Kim, H.-W. Progress in nanotheranostics based on mesoporous silica nanomaterial platforms. *ACS Appl. Mater. Interfaces* **2017**, *9*(12), 10309-10337.
49. Lee, C.H.; Lo, L.W.; Mou, C.Y.; Yang, C.S. Synthesis and characterization of positive-charge functionalized mesoporous silica nanoparticles for oral drug delivery of an anti-inflammatory drug. *Adv. Funct. Mater.* **2008**, *18*(20), 3283-3292.
50. Mohan, A.; Rout, L.; Thomas, A.M.; Nagappan, S.; Parambadath, S.; Park, S.S.; Ha, C.-S. Silver nanoparticles impregnated pH-responsive nanohybrid system for the catalytic reduction of dyes. *Microporous and Mesoporous Mater.* **2019**, *303*, 110260.
51. Moodley, T.; Singh, M. Polymeric mesoporous silica nanoparticles for enhanced delivery of 5-fluorouracil in vitro. Pharmaceutics **2019**, *11*(6), 288.
52. Saroj, S.; Rajput, S.J.; Tailor-made pH-sensitive polyacrylic acid functionalized mesoporous silica nanoparticles for efficient and controlled delivery of anti-cancer drug Etoposide. *Drug Dev. Ind. Pharm.* **2018**, *44*(7), 1198-1211.
53. Nechikkattu, R.; Park, S.S.; Ha, C.-S. Zwitterionic functionalised mesoporous silica nanoparticles for alendronate release. *Microporous and Mesoporous Mater.* **2019**, *279*, 117-127.
54. Santos, D.O.; Santos, M.L.N.; Costa, J.A.S.; Jesus, R.A.; Navickiene, S.; Sussuchi, E.M.; Mesquita, M.E. Investigating the potential of functionalized MCM-41 on adsorption of remazol red dye. *Environ. Sci. Pollut. Res.* **2013**, *20*(7), 5028-5035.
55. Liu, J.; Liu, S.; Li, Y.; Xue, J.; He, Y.; Liu, F.; Yang, L.; Hu, J.; Xiong, Z.; Long, L. Lanthanide-doped mesoporous MCM-41 nanoparticles as a novel optical–magnetic multifunctional nanobioprobe. *RSC Adv.* **2015**, *9*(70), 40835-40844.
56. Al-Thawabeia, R.A.; Hodali, H.A. Use of zeolite ZSM-5 for loading and release of 5-fluorouracil. *J. Chem.* **2015**, *2015*, Article ID 403597.
57. Park, S.S.; Jung, M.H.; Lee, Y.-S.; Bae, J.-H.; Kim, S.-H.; Ha, C.-S. Functionalised mesoporous silica nanoparticles with excellent cytotoxicity against various cancer cells for pH-responsive and controlled drug delivery. *Mater. Des.* **2019**, *184*, 108187.
58. Van Der Vis, M.; Cordfunke, E.; Konings, R. The thermodynamic properties of tetraethoxysilane (TEOS) and an infrared study of its thermal decomposition. *Le Journal de Physique IV* **1993**, *3*(C3), C3-75-C3-82.
59. Rosenholm, J.M.; Lindén, M. Wet-chemical analysis of surface concentration of accessible groups on different amino-functionalized mesoporous SBA-15 silicas. *Chem. Mater.* **2007**, *19*(20), 5023-5034.
60. Ulu, A.; Noma, S.A.A.; Koytepe, S.; Ates, B. Magnetic Fe_3O_4@ MCM-41 core–shell nanoparticles functionalized with thiol silane for efficient l-asparaginase immobilization. *Artif. Cells Nanomed. Biotechnol.* **2018**, *46*(sup2), 1035-1045.
61. Tham, W.; Chow, W.; Ishak, Z.M. The effect of 3-(trimethoxysilyl) propyl methacrylate on the mechanical, thermal, and morphological properties of poly (methyl methacrylate)/hydroxyapatite composites. *J. Appl. Polym. Sci.* **2010**, *118*(1), 218-228.
62. Vo, V.; Kim, H.-J.; Kim, H.-Y.; Kim, Y.; Kim, S.J. Synthesis of poly(methacrylic acid)-functionalized SBA-15 and its adsorption of phenol in aqueous media. *Bull. Korean Chem. Soc.* 2013, 34(12), 3570-3576.
63. Byler, D.M.; Farrell Jr, H.M. Infrared spectroscopic evidence for calcium ion interaction with carboxylate groups of casein. *J. Dairy Sci.* 1989, 72(7), 1719-1723.
64. Sing, K.S. Reporting physisorption data for gas/solid systems with special reference to the determination of surface area and porosity (Recommendations 1984). *Pure Appl. Chem.* **1985**, *57*(4), 603-619.
65. Mathew, A.; Parambadath, S.; Kim, S.Y.; Park, S.S.; Ha, C.-S. Adsorption of Cr(III) ions using 2-(ureylenemethyl)pyridine functionalized MCM-41. *J. Porous Mater.* **2015**, *22*(3), 831-842.
66. Hakeem, A.; Zahid, F.; Zhan, G.; Yi, P.; Yang, H.; Gan, L.; Yang, X. Polyaspartic acid-anchored mesoporous silica nanoparticles for pH-responsive doxorubicin release. *Int. J. Nanomedicine* **2016**, *13*, 1029-1040.
67. Saraswathy, M.; Stansbury, J.; Nair, D. Water dispersible siloxane nanogels: a novel technique to control surface characteristics and drug release kinetics. *J. Mater. Chem. B* **2016**, *4*(31), 5299-5307.
68. Tian, B.; Liu, S.; Wu, S.; Lu, W.; Wang, D.; Jin, L.; Hu, B.; Li, K.; Wang, Z.; Quan, Z. pH-responsive poly(acrylic acid)-gated mesoporous silica and its application in oral colon targeted drug delivery for doxorubicin. Colloids Surf. B **2017**, *154*, 287-296.
69. Ehi-Eromosele, C.; Ita, B.; Iweala, E. Silica coated LSMO magnetic nanoparticles for the pH-Responsive delivery of 5-Fluorouracil anticancer drug. *Colloids Surf. A Physicochem. Eng. Asp.* **2017**, *530*, 164-171.
70. Yuan, L.; Tang, Q.; Yang, D.; Zhang, J.Z.; Zhang, F.; Hu, J. Preparation of pH-responsive mesoporous silica nanoparticles and their application in controlled drug delivery. *J. Phys. Chem. C* **2011**, *115*(20), 9926-9932.
71. Peng, H.; Dong, R.; Wang, S.; Zhang, Z.; Luo, M.; Bai, C.; Zhao, Q.; Li, J.; Chen, L.; Xiong, H. A pH-responsive nano-carrier with mesoporous silica nanoparticles cores and poly(acrylic acid) shell-layers: fabrication, characterization and properties for controlled release of salidroside. *Int. J. Pharm.* **2013**, *446*(1-2), 153-159.
72. Moorthy, M.S.; Park, J.-H.; Bae, J.-H.; Kim, S.-H.; Ha, C.-S. Mesoporous organosilica hybrids with a tunable amphoteric framework for controlled drug delivery. *J. Mater. Chem. B* **2014**, *2*(38), 6487-6499.

 doi:10.20944/preprints202208.0066.v1

73. Wielińska, J.; Nowacki, A.; Liberek, B. 5-Fluorouracil-complete insight into its neutral and ionised forms. *Molecules* **2019**, *24*(20), 3683.
74. Li, H.; Yu, H.; Zhu, C.; Hu, J.; Du, M.; Zhang, F.; Yang, D. Cisplatin and doxorubicin dual-loaded mesoporous silica nanoparticles for controlled drug delivery. *RSC Adv.* **2016**, *6*(96), 94160-94169.
75. Nicotera, P.; Orrenius, S. The role of calcium in apoptosis. *Cell Calcium* **1998**, *23*(2-3), 173-180.